A&A 413, 257–272 (2004)
DOI: 10.1051/0004-6361:20031504
© ESO 2003

Astronomy & Astrophysics

Smoothed Particle Hydrodynamics simulations of merging white dwarfs⋆

J. Guerrero[1], E. García–Berro[1,2], and J. Isern[1,3]

[1] Institute for Space Studies of Catalonia, c/Gran Capitá 2–4, Edif. Nexus 104, 08034 Barcelona, Spain
[2] Departament de Física Aplicada, Escola Politécnica Superior de Castelldefels, Universitat Politécnica de Catalunya, Avda. del Canal Olímpic s/n, 08860 Castelldefels, Spain
[3] Institut de Ciéncies de l'Espai, C.S.I.C.

Received 4 July 2002 / Accepted 4 September 2003

Abstract. We present the results of three-dimensional Smoothed Particle Hydrodynamics (SPH) calculations of the process of coalescence of white dwarfs. We follow in detail the initial phase of the merging for several masses of the primary and the secondary of the binary system. Special attention has been paid to the issue of whether or not thermonuclear runaway occurs during the process of merging. We find that although relatively high temperatures are attained during the most violent phase of the merging process, the thermonuclear flash is rapidly quenched. The total mass lost by the system is also relatively small (of the order of 0.5% at most) except for the most massive primaries for which it is still small (~2.2%). Consequently, a heavy accretion disk around the primary is formed. We also discuss the subsequent evolution of the resulting system and the possible astrophysical scenarios of interest.

Key words. stars: white dwarfs – stars: interiors – stars: binaries: close – hydrodynamics – methods: numerical – accretion, accretion disks

1. Introduction

The merging of two white dwarfs is the final destiny of a good fraction of binary systems. The process of formation of such systems involves two mass transfer episodes of the progenitor stars when each of the components of the binary system evolves off the main sequence. Although the astrophysical scenarios in which a merging of two white dwarfs in a close binary system can occur and their relative frequencies has been relatively well studied – see, for instance, Yungelson et al. (1994), and Nelemans et al. (2001a, 2001b), and references therein – the process of merging itself has received little attention. The only exceptions are the works of Mochkovitch & Livio (1989, 1990) who used an approximate method – the so-called Self-Consistent-Field method (Clemens 1974) – and the full SPH simulations of Benz et al. (1989), Benz et al. (1990), and Segretain et al. (1997). Benz et al. (1989) studied the collisions of two white dwarfs of masses $0.6 + 0.6\,M_\odot$ and $0.7 + 0.9\,M_\odot$ respectively, for several impact parameters, taking into account the effects of nuclear reactions, but using a reduced resolution (only 5000 particles were used), whereas Benz et al. (1990) studied the process of dynamic mass exchange in a $0.9 + 1.2\,M_\odot$ binary system, but they did not take into account the effect of nuclear reactions. On the other hand, Benz et al. (1989) included these effects but they did not discuss the merged configuration. Finally, Segretain et al. (1997) studied only the coalescence of a $0.6+0.9\,M_\odot$ white dwarf pair, but they did not take into account the effect of nuclear reactions, although they paid close attention to the merged configuration. It is worth noticing at this point that in all these simulations but the last one, the classical expression for the artificial viscosity – see, for instance, Monaghan & Gingold (1983) – was used. It is a well known fact that SPH induces a large shear viscosity, which is more pronounced when the classical expression for the artificial viscosity is used. However there are more recent formulations of the artificial viscosity which reduce considerably the excess of shear dissipated (Balsara 1995). In summary, the available simulations cover a very small range of masses and chemical compositions of the white dwarfs involved in the merger. Additionally, some of them do not study the effect of nuclear reactions and, finally, all of them but the most recent one do not use an appropiate formulation of the artificial viscosity. Indeed, one of the probable reasons for this lack of theoretical models is the heavy computational demand involved in the simulation of an intrinsically three-dimensional phenomenon. However, in sharp contrast, the coalescence of two neutron stars has been extensively studied – see, for instance, Rosswog et al. (2001) and Rosswog & Davies (2000, 2002),

Send offprint requests to: E. García–Berro,
e-mail: garcia@fa.upc.es
⋆ Figures 2, 4, 6, 7 are only available in electronic form at http://www.edpsciences.org

Article published by EDP Sciences and available at http://www.aanda.org or http://dx.doi.org/10.1051/0004-6361:20031504

and references therein, for some of the most recent works on this subject.

There are several reasons for studying the coalescence of two white dwarfs. Firstly it should be noted that the double degenerate scenario (Webbink 1984; Iben & Tutukov 1984), in which the merging of two carbon–oxygen white dwarfs with total mass larger than the Chandrasekhar limit occurs, has been one of the most favored scenarios leading to type Ia supernovae. Although this scenario is not currently the preferred one, it is still worth studying it since it is not yet clear whether or not carbon burning may occur during the impact of the material of the disrupted secondary onto the surface of the massive primary for the whole range of masses of both stars involved in the merging process. Moreover, it has been recently suggested that such a process would lead to both a type Ia supernova explosion and to the formation of a magnetar (King et al. 2001). This scenario would explain the main characteristics of soft gamma-ray repeaters and anomalous X-ray pulsars like 1E2259+586. This enigmatic X-ray pulsar, has an unusually soft spectrum, an unusually stable period with a very stable and positive value of the period derivative and it seems to be a single star, and it has been interpreted as the outcome of a recent merger of two white dwarfs (Paczynski 1990).

Secondly, it has been also suggested (Schmidt et al. 1992; Segretain et al. 1997) that three hot and massive white dwarfs (PG 0136+251, PG 1658+441 and GD 50), presumably members of the galactic halo, could be the result of the coalescence of white dwarfs. Finally, the initial stages of the coalescence of a white dwarf binary system could be one of the most interesting sources for the detection of gravitational waves using Earth-based laser interferometers like LIGO (Abramovici et al. 1992) or space-borne detectors like LISA (`http://lisa.jpl.nasa.gov`). In particular, Galactic close binary white dwarfs are expected to contribute significantly to the background noise (Evans et al. 1987) during the spiraling phase and the merging process itself would produce a signal that could eventually be detected (Seto 2002).

Finally, it is worth mentioning that during the last decade several observational programs (Bragaglia et al. 1990; Marsh 1995; Marsh et al. 1995; Maxted & Marsh 1999) have been conducted in order to find double degenerates with orbital periods small enough (of the order of a few hours) such as to merge within a Hubble time, and massive enough so as to exceed the Chandrasekhar limit. These searches have yielded at last one potential candidate with such characteristics, the pulsating sdB star KPD 1930+2752 (Maxted et al. 2000). This star is member of a binary system with a total mass of 1.47 $M_\odot$, which will merge within ∼200 million years. Hence, at least one possible precursor of these kind of systems now exists.

In this paper we present the results of SPH calculations of merging white dwarfs. We have explored a wide range for the masses of both components. In particular we have studied the following cases: 0.4 + 0.4 $M_\odot$, 0.4 + 0.6 $M_\odot$, 0.6 + 0.8 $M_\odot$, 0.6 + 1.0 $M_\odot$, 0.8 + 1.0 $M_\odot$, and 1.2 + 0.4 $M_\odot$. However, and for the sake of conciseness, our discussion will be centered around the most significative cases. That is, we will describe in detail the merger of a 0.6 + 0.8 $M_\odot$ pair, since in this case the two merging white dwarfs are made of carbon and oxygen, and the total mass of the system is larger than the Chandrasekhar limit. We will also discuss in some detail the merger of a low mass system in which the two components are made of helium (the 0.4 + 0.4 $M_\odot$ case), and the merger of a 1.2 + 0.4 $M_\odot$ system, in which a massive oxygen-neon white dwarf and a light white dwarf made of helium and, hence, with a small Coulomb barrier, are involved. We will pay special attention to this last simulation because this would be the case in which a thermonuclear flash could eventually develop most easily. Finally, we will also discuss in detail the coalescence of a 0.4 + 0.6 $M_\odot$ pair because this is the case in which an otherwise typical carbon-oxygen white dwarf and a light-weight helium white dwarf are involved. It is worth mentioning at this point that although we will not discuss in full detail all the simulations presented here, they can be found in mpeg format at the following URL: `ftp://ftp.ieec.fcr.es/pub/astrofisica/SPH`. The paper is organized as follows. In Sect. 2 we briefly describe our input physics and the method of calculation. In Sect. 3 we present the results for all the cases discussed above and, in less detail, the rest of the cases in which carbon-oxygen white dwarfs are involved. Finally in Sect. 4 we summarize our results and draw our conclusions.

2. Input physics and method of calculation

We follow the hydrodynamic evolution of the binary system using a Lagrangian particle numerical code, the so-called Smoothed Particle Hydrodynamics. This method was first proposed by Lucy (1977) and, independently, by Gingold & Monaghan (1977). The fact that the method is totally Lagrangian and does not require a grid makes it specially suitable for studying an intrinsically three-dimensional problem like the coalescence of two white dwarfs. We will not describe in detail the most basic equations of our numerical code, since this is a well-known technique. Instead, the reader is referred to Benz (1990) where the basic numerical scheme for solving the hydrodynamic equations can be found. Our SPH code follows very closely this scheme. However and for the sake of completeness we shortly describe the most important physical ingredients incorporated into the numerical code.

We use the standard polynomic kernel of Monaghan & Lattanzio (1985). The gravitational forces are evaluated using an octree (Barnes & Hut 1986). The artificial viscosity adopted in this work is that of Balsara (1995) and it is only important in the presence of shocks. Regarding the integration method we use a predictor-corrector numerical scheme with variable time step (Serna et al. 1996), which turns out to be quite accurate. With this integrator the energy and angular momentum of the system are conserved to a good accuracy (of the order of 10^{-4} over 10^4 time steps) with relatively large time-steps.

The equation of state adopted for this work is the sum of three components. The ions are treated as an ideal gas but taking into account the Coulomb corrections. We have also incorporated the pressure of photons, which turns out to be important only when nuclear reactions become relevant (see Sect. 3). Finally the most important contribution is the pressure of degenerate electrons which is treated as the standard zero temperature expression plus the temperature corrections. The nuclear

network adopted here (Benz et al. 1989) incorporates 14 nuclei: He, C, O, Ne, Mg, Si, S, Ar, Ca, Ti, Cr, Fe, Ni and Zn. The reactions considered are captures of α particles, and the associated back reactions, the fussion of two C nuclei, and the reaction between C and O nuclei. All the rates are taken from Rauscher & Thielemann (2000). The nuclear energy release is computed independently of the dynamical evolution with much smaller time-steps, assuming that the dynamical variables do not change much during these time-steps.

The thermal evolution of the system is followed in two ways. On the one hand the variation of the internal energy is followed according to:

$$\frac{\mathrm{d}u_i}{\mathrm{d}t} = \frac{P_i}{\rho_i^2} \sum_{j=1}^{N} m_j \boldsymbol{v_{ij}} \boldsymbol{\nabla_i} W(r_{ij}, h) \tag{1}$$

where $W(r_{ij}, h)$ is the smoothing kernel and the rest of the symbols have their usual meaning. On the other, we simultaneously compute the temperature variation according to:

$$\frac{\mathrm{d}T_i}{\mathrm{d}t} = -\sum_{j=1}^{N} \frac{m_j}{(C_\mathrm{v})_j} \frac{T_j}{\rho_i \rho_j} \left[\left(\frac{\partial P}{\partial t}\right)_\rho\right]_j \boldsymbol{v_{ij}} \boldsymbol{\nabla_i} W(r_{ij}, h). \tag{2}$$

If in the region under study the temperature is below 6×10^8 K or the density is smaller than 6×10^3 g/cm^3 we use Eq. (2) otherwise we use Eq. (1). We have found that in this way energy is better conserved.

In order to achieve an equilibrium initial configuration we relaxed each individual model star separately. In all cases the initial system is composed of the two white dwarfs in a circular orbit at a distance larger than the corresponding Roche lobe radius of the less massive component. To this system we add a very small artificial acceleration term which decreases the separation of both components. Once the secondary fills its Roche lobe this acceleration term is supressed. We adopt this instant as our time origin. The system is not synchronized because, at least in the stage previous to the coalescence itself, the time scale for loss of angular momentum due to the emission of gravitational radiation is so small that it remains quite unlikely that there exists any dissipation mechanism able to ensure synchronization (Segretain et al. 1997). Of course with this approach the initial configurations of both the primary and the secondary have small departures from sphericity due to tidal forces. These departures become more prominent as time passes by, as it will be shown in Sect. 3 below. The typical number of particles for each white dwarf is 2×10^4, a factor of 4 larger than in Benz et al. (1989) and of the same order than that used by Segretain et al. (1997).

3. Results

3.1. CO+CO mergers

As previously explained we will only discuss in detail the evolution of the $0.6 + 0.8\,M_\odot$ system. The other two cases will be shown in less detail. In Fig. 1 we show the temporal evolution of the positions of the SPH particles as a function of time for the $0.6 + 0.8\,M_\odot$ system. The time for each panel is clearly indicated in the upper left corner of each panel in code units, which results from adopting $1\,M_\odot$ as mass unit, $0.1\,R_\odot$ as length unit and taking $G = 1$, and which turns out to be about 50 s. As it can be seen in this figure, the initial configuration is almost completely spherically symmetric. After some time the secondary has overflown its Roche lobe and an accretion stream forms. This accretion stream is directed towards the primary, forming an arm. The particles flowing from the secondary onto the primary are redistributed over the surface of the primary and the arm twists as time increases, leading to the formation of a heavy accretion disk with cylindrical symmetry. The whole process lasts for about one minute. This is due to the positive feedback experienced by the secondary: as the coalescence proceeds the secondary losses mass and, thus, becomes less dense and expands leading to an enhanced mass-loss rate which, in turn, leads to a decrease of the average density of the secondary.

In Fig. 2 we show the evolution of the velocity field as seen from the reference frame of the center of masses of the system of those particles with z coordinate in the range $-0.003 \leq z \leq 0.003$ code units (1 code unit is $= 0.1\,R_\odot$), that is, those particles close to the orbital plane. This value is relatively arbitrary, as long as it is much smaller than the size of the system (~0.1 code units) and, simultaneously, it is large enough so that there is a significant number of particles in it (of the order of 10^3). In this way we make sure that we are selecting a statistically significant number of particles belonging to the orbital plane. In the top left panel of Fig. 2 (corresponding to $t = 0$) we can see that all the particles have the same rotational velocity and, hence, none of the stars rotates around its own axis. The formation of the accretion arm is clearly seen in the top right panel. This arm is primarily composed of high velocity particles. However, it can also be observed that the particles which are closer to the primary have smaller rotation velocities. This is a consequence of the dissipation due to the artificial viscosity which will be discussed below. But, on the other hand, the particles belonging to the outer edge of the accretion arm have larger velocities and ultimately will be ejected from the system. The left central panel of Fig. 2 shows how the particles of the secondary accumulate onto the primary. The right central panel shows that at this point of the evolution the particles coming from the secondary already have a very small radial velocity and, consequently, that there is a substantial circularization of the orbits. Moreover, the accretion disk is supported by its own rotational velocity. However, we can still find a spiral pattern which becomes less and less apparent as time increases, reaching cylindrical symmetry during the very late stages of the simulation (bottom panels). In fact, the accretion rate becomes negligible during this phase. The final number of particles that are ejected from the system is very small (see Table 1), and correspondingly only 0.2% of the total mass of the system is lost during the coalescence process. Most of this particles are ejected during the first and most violent phase of the merger.

In Fig. 3 the evolution of the average tangential velocity and their corresponding dispersions (at 2σ) with respect to the center of mass reference frame are shown. The abcissa is the cylindrical radius measured from the center of the primary. In the top left panel it can be seen how the rotation velocity of the

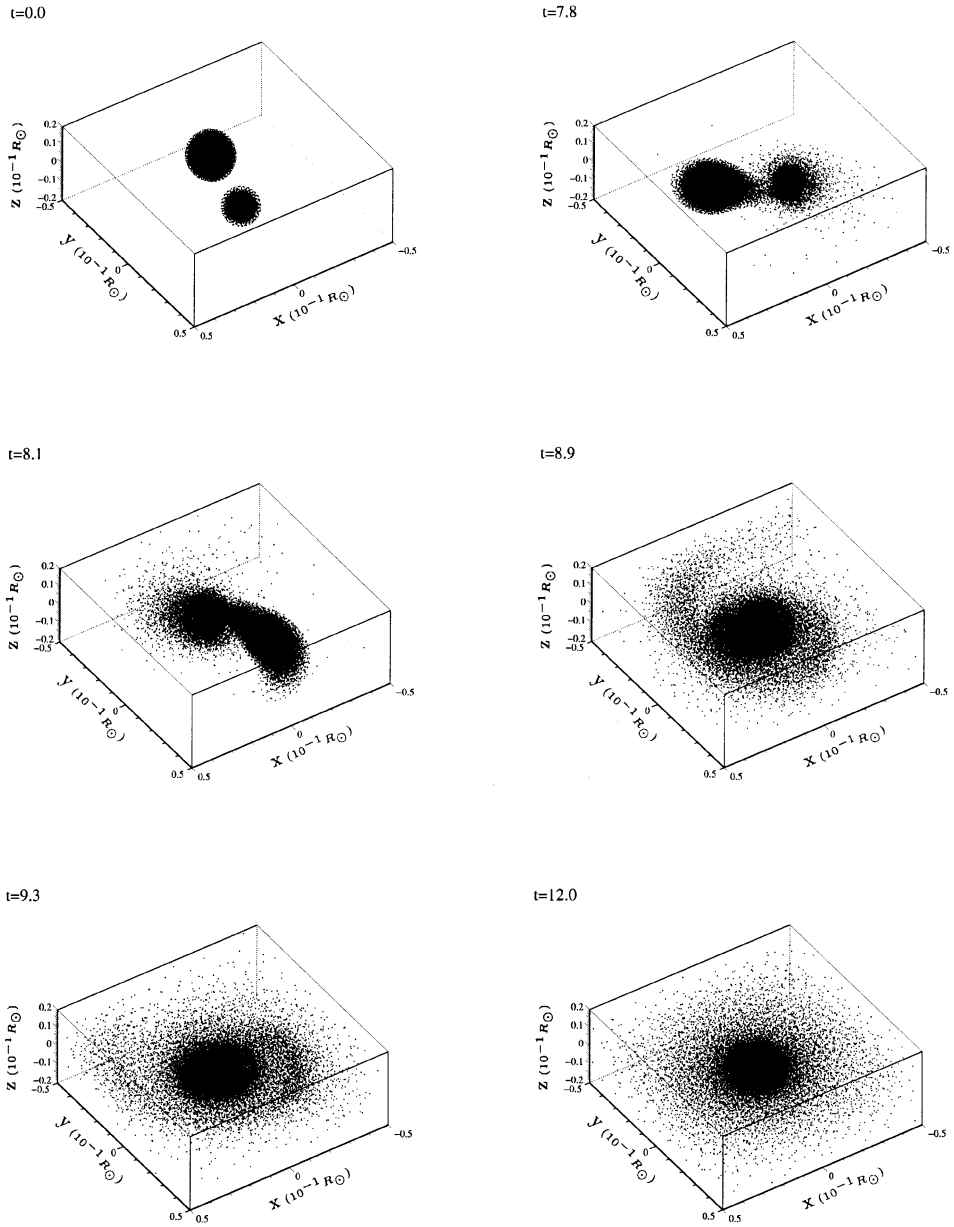

Fig. 1. Temporal evolution of the positions of the SPH particles for the 0.6 + 0.8 $M_\odot$ system. Time is shown – in code units – in the upper left corner of each panel.

particles is essentially the orbital velocity of both stars. Due to the tidal forces the dispersions are larger for the regions of the secondary closer to the primary. In the next panel it can be seen how a region with $0.1 \leq r_{\rm cyl} \leq 0.25$ develops very large dispersions, which are caused by the collision of the spiral arm with the surface of the primary. It is noticeable that the value of the tangential velocity of this region remains more or less constant during the whole simulation. The Keplerian rotational velocity at a distance 0.15 code units ($\simeq 1.5 \times 10^{-2}\, R_\odot$) for a 0.8 $M_\odot$ central object is 2.3 code units (about 3.2×10^3 km s^{-1}), which is the average value of the rotational velocity of the particles within this region. Hence, the particles in this region have on average a Keplerian rotation velocity and the circular orbit is stable. Since in the end an accretion disk forms, and the accretion rate is relatively small, it is natural to find that this velocity remains almost constant. In the central right panel of this figure we see how the rotational velocity of the primary increases as a consequence of (i) the transfer of orbital angular momentum to rotational angular momentum due to the accreted matter and, (ii) the effect of the artificial viscosity.

SPH numerical codes are known to be affected by a large shear viscosity which results in artificial kinetic energy dissipation in shear flows. We have used the artificial viscosity of Balsara (1995), which does not produce an excessive shear and, consequently, reduces somewhat (but not completely) these problems. It is obvious from the bottom panels of Fig. 3 that shear dissipation exists, since we see that by the end of the merger the primary already rotates as a rigid solid, which is what one may expect for a viscous fluid, whereas the accretion disk has a flat profile with very small dispersion. However, it

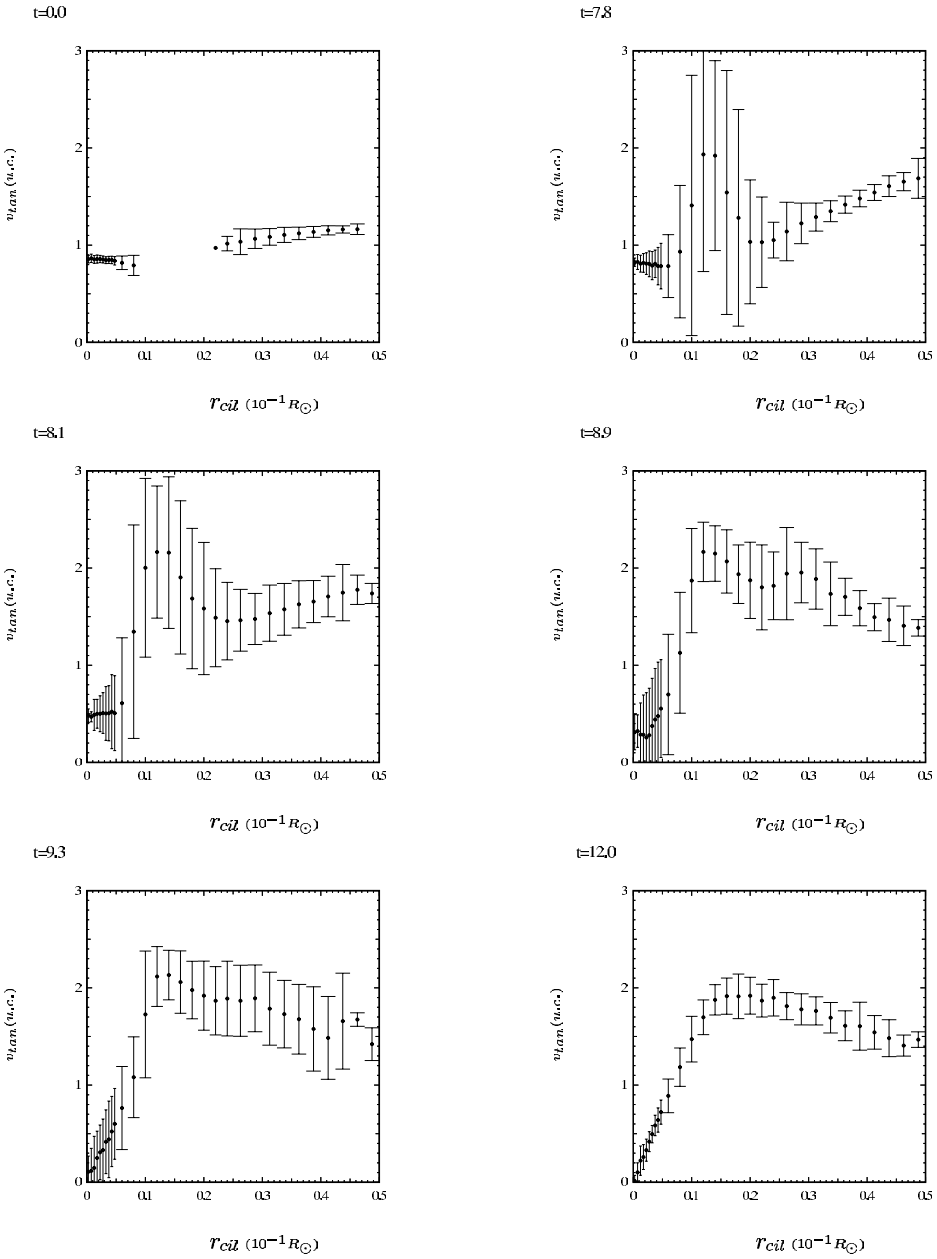

Fig. 3. Temporal evolution of the tangential velocity with respect to center of mass reference frame of the SPH particles for the $0.6+0.8\ M_\odot$ system. Time is shown – in code units – in the upper left corner of each panel.

is clear that in absence of viscous or gravitational torques the primary should not be spun up. As it can be seen in Fig. 3 the primary is spun up to solid rigid rotation with an angular velocity $\omega = 0.3\,\mathrm{s}^{-1}$ in about 1 min. Hence, it is quite likely that the rotational velocities of the central object obtained here are overestimates. It is important to realize that this unphysical spinning up of the primary represents both a significant dissipation rate ($\approx 10^{47}$ erg/s) and an angular momentum sink. Therefore, some properties of the merged object could be affected by the excess of rotation of the primary. Thus, even if we use the artificial viscosity of Balsara (1995) the final configuration could not be reliable. Note that the problem of the coalescence of white dwarfs has been previously studied by Benz et al. (1990). These authors used a reduced resolution (3000 particles were used in their simulations) and the classical expression for the artificial viscosity. Therefore, our simulations should produce more accurate results. However, the unphysical shear componenent does not decrease with increasing resolution. In fact, resolution only affects the width of the region in which this extra dissipation occurs. Since linear resolution scales as $N^{1/3}$, this region is typically two times smaller in our simulations when compared with those of Benz et al. (1990). The dissipation of kinetic energy will most probably translate into an overestimate of the resulting temperature profiles (see below). However, given the resolution used in our calculations and the smearing due to artificial viscosity – which leads to an underestimate of the temperature in the shocked regions – it is difficult to ascertain which effect is most important. Nevertheless, since the maximum temperatures are achieved during the very early stages of the merging process it is quite probable that these

Table 1. Global parameters of the simulations of the CO+CO mergers.

Simulation	0.6+0.8	0.6+1.0	0.8+1.0
Ratio	0.75	0.60	0.80
$T_{\max}$ (K)	1.4×10^9	1.6×10^9	2.0×10^9
Mass of the particles ($M_\odot$)	3×10^{-5}	3×10^{-5}	4×10^{-5}
Expelled particles	94	216	163
Expelled mass ($M_\odot$)	2.82×10^{-3}	6.48×10^{-3}	6.52×10^{-3}
Fraction of the secondary expelled	4.7×10^{-3}	1.1×10^{-2}	8.2×10^{-3}
Total expelled fraction	2.0×10^{-3}	4.0×10^{-3}	3.6×10^{-3}
Duration (s)	50	65	20

temperatures are indeed overestimates of the real ones. This is the reason why from now on we will mostly focus on the early stages of the coalescence. However, it is worth noticing that our calculations represent a clear improvement with respect to those of Benz et al. (1990) since we use an improved treatment of the artificial viscosity and an enhanced resolution. Additionally, we cover a range of masses and chemical compositions wider than those of Segretain et al. (1997) and we also take into account the effects of nuclear reactions, which were disregarded in their work.

Finally, in Fig. 4, the evolution of the temperature in the orbital plane is shown. The contours represented in this figure are logarithmic but the scale is linear. In the top $x-y$ plane the positions of the particles projected in the orbital plane are shown as a visual aid. The first of these panels shows the initial state of the system with the adopted initial temperature of 10^7 K. In the second panel we can see that the temperatures of both the primary and the secondary have increased considerably as consequence of the impact of the accretion arm. The local maximum clearly seen in the lower left corner of this figure corresponds to a single particle (see the top $x-y$ plane) and, hence, it should be disregarded since it is not statistically significant. In the region were the impact occurs the temperature is now 3×10^8 K. In the next panel the temperature of the hot spot is now slightly larger than 10^9 K and, hence, some material is burnt. Nevertheless a strong thermonuclear flash does not develop because the temperature in this region increases very rapidly, lifts degeneracy and expands the material, quenching the thermonuclear flash. The final object is hot ($\sim 5 \times 10^8$ K) and has a characteristic volcano shape with the region of maximum temperature located in the region between the accretion disk and the primary. As discussed previously, the kind of numerical technique we are using has probably led us to overestimate the temperature in the regions were a shock occurs. Note that even though we are probably overestimating the temperatures, the thermonuclear flash never fully develops. Therefore, it is unlikely that the coalescence of the white dwarf pair will lead to an explosion, although we cannot totally discard it.

In Table 1 we have summarized the most relevant results of the three simulations for the range of masses of the binary system studied here. In the first row of this table the ratio of masses is shown, whereas in the second row the maximum temperature attained during the merger can be found. The third row shows the mass of the particles used in the simulation. In the fourth row the number of particles expelled from the system after the whole process of coalescence is over can be found. In the fith, the sixth and the seventh rows we show the ejected mass, the fraction of the secondary ejected during the merger, and the total ejected fraction. Finally, the last row shows the total duration of the merger (in s) measured from the moment at which the first impact of the spiral arm onto the primary occurs until the moment at which the spiral arm disappears. Clearly the maximum temperature attained during the process of coalescence increases with the mass of the primary and the secondary. As it can be seen in Fig. 4, the maximum temperature is attained during the first contact of the spiral arm with the primary and results from the conversion of kinetic energy into thermal energy. Obvioulsy the more massive the primary is the stronger is the shock. Besides, the more massive is the primary the smaller its radius is and, consequently, the particles of the secondary have more time to be accelerated before the collision with the surface of the primary and, hence, more kinetic energy is available. Also, it is interesting to see that the more massive the secondary is the higher the maximum temperature is. This is due to the fact that more mass per unit time is accreted in a more or less constant time interval. Nevertheless we emphasize that none of the maximum temperatures, which as already discussed have been probably overestimated, is large enough to produce a supernova explosion during the coalescence.

The second important point is the mass ejected from the system. This mass turns out to be very small for all the three cases studied here. In all these simulations the mass is ejected from the secondary and, moreover, most of the particles are ejected during the first impact of the spiral arm onto the surface of the primary. An analysis of Table 1 shows that the ejected mass increases with the ratio of masses. Again, this behavior can be easily explained taking into account that when the masses of both white dwarfs are similar the region where the impact occurs is closer to the center of masses of the system and, secondly, that massive white dwarfs have smaller radii and, consequently, the particles of the secondary obtain larger kinetic energies. Finally, the total duration of the merger is similar in all three cases and there is no clear dependence on either the mass of the primary nor the ratio of masses.

3.2. He+He, He+ONe and He+CO mergers

3.2.1. He+He mergers

In Fig. 5 the result of the coalescence of two $0.4\,M_\odot$ white dwarfs is shown. The top left panel shows how both stars begin to overflow their respective Roche lobes as a consequence

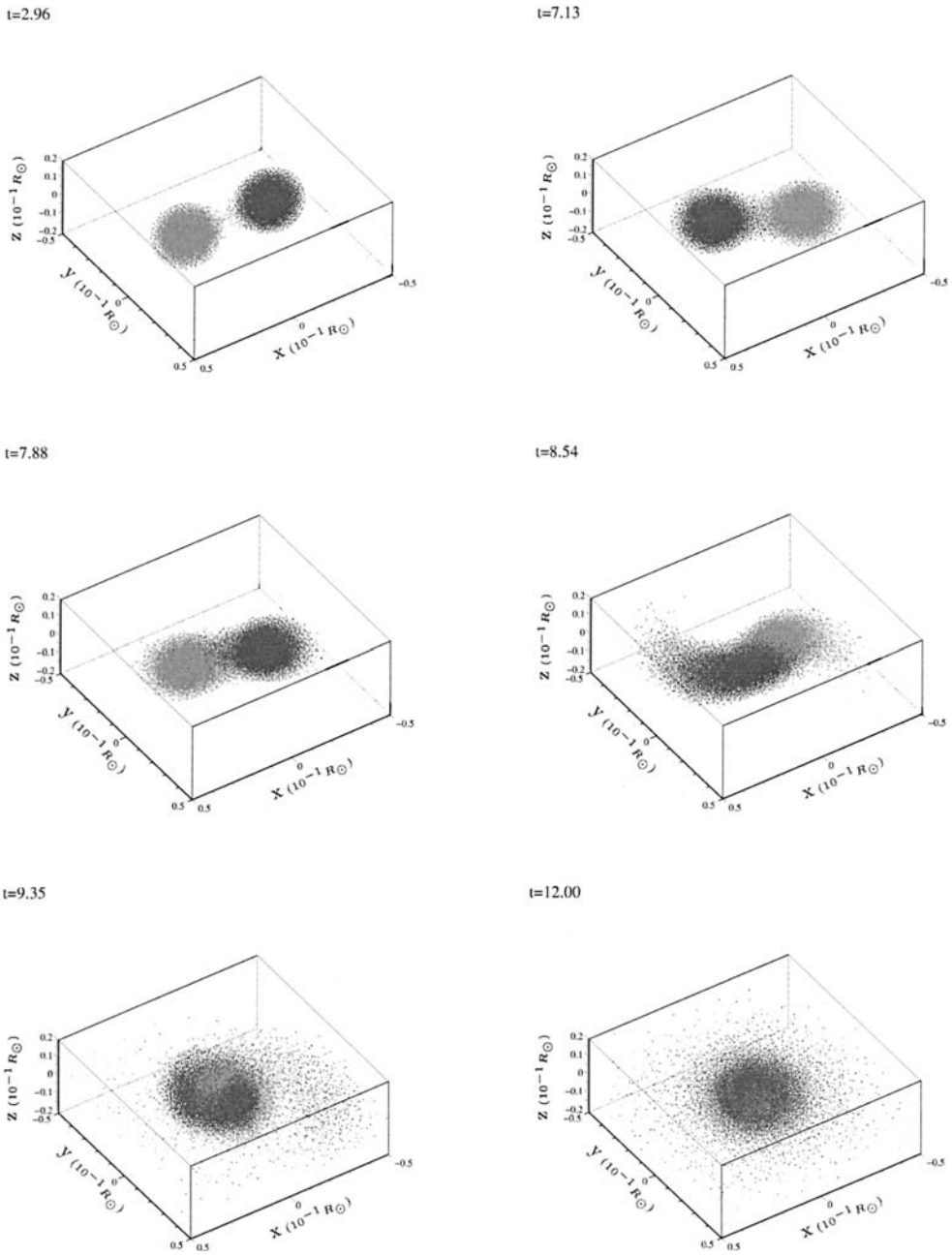

Fig. 5. Temporal evolution of the positions of the SPH particles for the 0.4 + 0.4 $M_\odot$ system.

of tidal interactions. This is even more clear in the top right panel and in the central left panel where the symmetry is still preserved. At a certain point of the simulation, two spiral accretion streams are formed (middle right panel). The density of the streams is relatively small. These streams are slightly different, depending on the orbital phase at which they form. Note that at the center of masses a shocked region forms as a consequence of the impact between both streams. By the end of the simulation (bottom panels) both streams become entangled and the configuration of the resulting objects consists in a central region where the particles coming from one of the original objects dominate whereas in the outer regions the particles coming from the other are more abundant. No mass is ejected from the system. The resulting object has cylindrical symmetry and spins around its axis.

In Fig. 6 the velocity fields found for this simulation are shown. Again it is easy to see how these spiral accretion streams are formed, and how symmetry is broken during the central phases of the coalescence process, although it is finally recovered by the end of the simulation. It is interesting to note (central panels) that during the central phases of the coalescence the particles of the most external layers of both stars still have basically their orbital velocities, whereas the central regions already have a complex whirlpool structure which will be maintained until the end of the simulation. It is also worth observing that during this phase the velocity vectors do not have significant radial components. Hence, even during the most violent phase of the simulation, mass loss is negligible. Morever in the central region a bar-like oblique shock forms as a consequence of the discontinuity in the velocity field.

The hot bar-like structure is located at the interface between the two bodies, where a severe shear layer exists. The simulations of merging neutron stars (Rosswog & Davies 2002) have shown that this shear layer develops vortices as it is subject to Kelvin-Helmholtz instabilities. Given our resolution we cannot resolve them. Moreover the excess shear introduced by our treatment of the artificial viscosity transforms these vortices in a hot contact region which appears as a hot bar.

The succesive panels of Fig. 7 show the temporal evolution of the equatorial temperature profiles and the projected positions of the SPH particles. At the beginning of the simulation (top left panel) both stars are almost isothermal ($T \sim 10^7$ K), except for the most external regions which have already expanded and cooled. In the top right panel of Fig. 7 it already appears the most significant trend in this simulation, namely the existence of the bar-like structure in the contact region between the spiral accretion streams. This bar-like structure initially has a temperature slightly larger than the surrounding areas. As time passes by the temperature in this region remarkably increases (middle panels) and, ultimately, the shape of this bar becomes curved (bottom left panel) as a consequence of the mass transfer process. Finally, by the end of the simulations, the temperature of the resulting object has axial symmetry, the maximum of temperatures being located in the central regions (bottom right panel). Nevertheless the maximum temperature achieved during the simulation (2×10^8 K) is not enough to drive a thermonuclear flash able to eject mass from the system or to trigger an explosion but, instead, drives an expansion (and cooling) of the most external layers. By the end of the simulation the temperature has decreased considerably to a value of 1.6×10^8 K.

3.2.2. ONe+He mergers

In Fig. 8 the temporal evolution of the three-dimensional positions of the SPH particles are shown for the case of merger of the $1.2+0.4\,M_\odot$ binary system. For this case the primary is very compact and, hence, the coalescence process is rather violent. This can be clearly seen in the top panels of this figure, were the almost instantaneous disruption of the secondary can be observed. In fact most of the particles of the secondary form an accretion stream which collides with the compact surface of the primary and bounces back. Some of these reflected particles are quite apparent in the top right panel of Fig. 8. As the process of merging proceeds the accretion arm is totally reflected (left middle panel) and finally forms an extended toroidal estructure around the ONe primary. However, this structure lasts only for a few moments and finally another (more extended) accretion stream is formed, which again hits the surface of the primary leading to the formation of the accretion disk which has been found in the simulations described in Sect. 3.1.

In order to better visualize the structure of the resulting object, in Fig. 9 the axial density profiles for azimuthal angles ranging from 0° to 150° in 30° intervals are shown. As it is clear from a superficial inspection of this figure, the accretion disk is far from being uniform and, in fact, still has some spiral structure. Following the panels from top to bottom and from left to right, respectively, we see that the accretion arm is hitting the surface of the primary. This accretion arm extends all over the equatorial plane and surrounds the primary at increasing distances as we move around the primary. The variations of the density within the disk are of up to $\simeq$50%. Thus, the disk still presents some inhomogeneities which can be attributed to the succesive reflections of the accretion stream. However for large enough times these irregularities eventually disappear and the particles in the disk acquire Keplerian orbits.

The temporal evolution of the structure of the velocity field is shown in Fig. 10. This figure clearly shows how the secondary is disrupted in a dynamical time scale forming an accretion stream that impacts the surface of the primary (top panels). Note the very large velocities of the reflected particles. This particles will be ejected from the system in succesive passages of the accretion arm. The total ejected mass for this simulation is relatively high when compared with the mass ejected in less massive primaries, of the order of $3.54\times10^{-2}\,M_\odot$, which represents a 2.2% of the mass of the system and a ∼9% of the mass of the secondary – all the particles ejected from the system belong to the destroyed secondary. It also helps in visualizing the formation of the toroidal structure previously discussed (middle right panel). And, finally, clearly shows as well how by the end of the simulation the SPH particles form a Keplerian accretion disk (bottom panels).

Finally, in Fig. 11 the evolution of the equatorial temperature profiles is displayed. The initial configuration, as usual, presents isothermal profiles. When the first particles of the secondary impact the surface of the primary (top right panel), the temperature in the shocked regions reaches a maximum of $\sim5 \times 10^8$ K. However, this region is very small and, almost instantaneously, the colliding particles are reflected by the hard boundary of the compact primary. At this point of the evolution the bulk of the secondary star has not changed appreciably its temperature. In the central panels of this figure it is clearly shown how as the mass transfer process proceeds the accreted matter is shocked and heated on top of the surface of the primary (left middle panel) but, as the evolution continues, this matter is expelled from the surface of the primary and a hot toroidal structure forms (right middle panel). The temperatures are in both cases in excess of 10^9 K and nuclear reactions transform the accreted He in C and O. However, the thermonuclear flash is rapidly quenched and the nuclear reactions never proceed so fast as to be able to produce a thermal avalanche. It is worth mentioning at this point again that due to the numerical treatment we are using these temperatures have been probably overestimated and, consequently, the possibility of a supernova explosion by means of what it can be called a direct impact, remains unlikely.

3.2.3. CO+He mergers

In Fig. 12 the temporal evolution of the three-dimensional positions of the SPH particles are shown for the case of merger of the $0.6 + 0.4\,M_\odot$ binary system. As it was the case for the $0.8 + 0.6\,M_\odot$ merger, a narrow accretion stream forms as a consequence of the tidal interaction between both components of

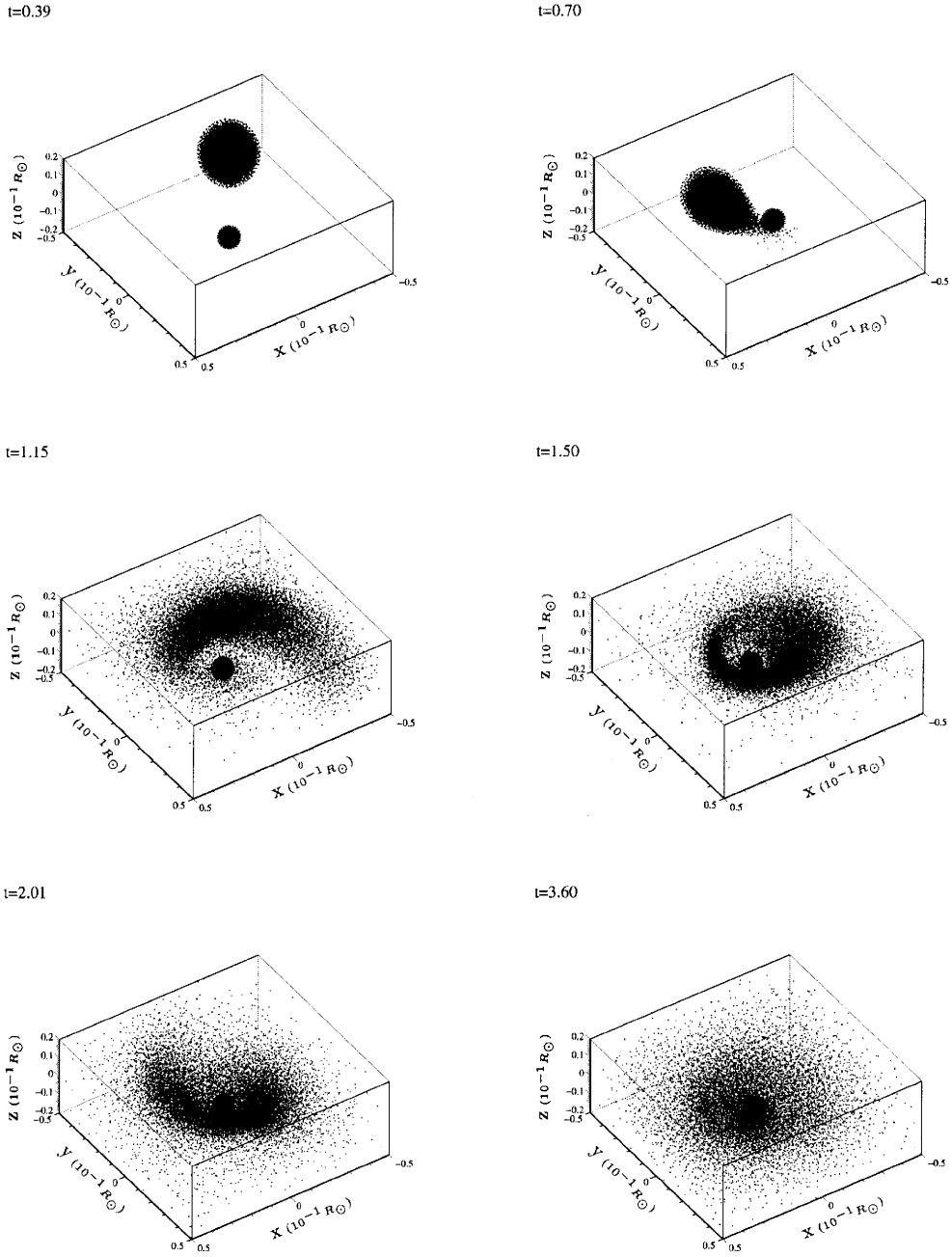

Fig. 8. Temporal evolution of the positions of the SPH particles for the 1.2 + 0.4 $M_{\odot}$ system.

the binary system. Note that, as expected, the primary is not significantly deformed whereas the secondary is considerably deformed (top right panel). As time goes on the bulk of the mass of the secondary is rapidly swallowed by the primary (central panels) and, ultimately, an accretion arm and later an accretion disk are formed very much in the same way as it was previously described in Sect. 3.1. The temporal evolution of the velocities projected on the orbital plane is shown in Fig. 13. Again the formation of the narrow accretion stream is clearly shown in the top right panel of this figure. Note as well that as a consequence of the impact of the particles of the secondary onto the surface of the primary an spiral arm is formed (middle panels) which later evolves forming a heavy accretion disk (bottom panels). Finally, in Fig. 14 the evolution of the temperature profiles is shown. Again a region of high temperatures is formed around the equatorial plane of the primary. These regions reach a considerably high temperature and, consequently, some material is burnt. In this case due to the different chemical composition of the merging white dwarfs most of the energy is released as a consequence of the $C^{12}(\alpha,\gamma)O^{16}$ reactions. Nevertheless the temperatures achieved are not extremely high and, as it was found in all the cases studied so far in this paper, degeneracy is rapidly lifted, the regions were some material is burnt consequently expand and the thermonuclear runaway is ultimately quenched. We emphasize again that due to our numerical treatment of the artificial viscosity the resulting temperatures have been probably overstimated. Hence, even in the case in which a light white dwarf made

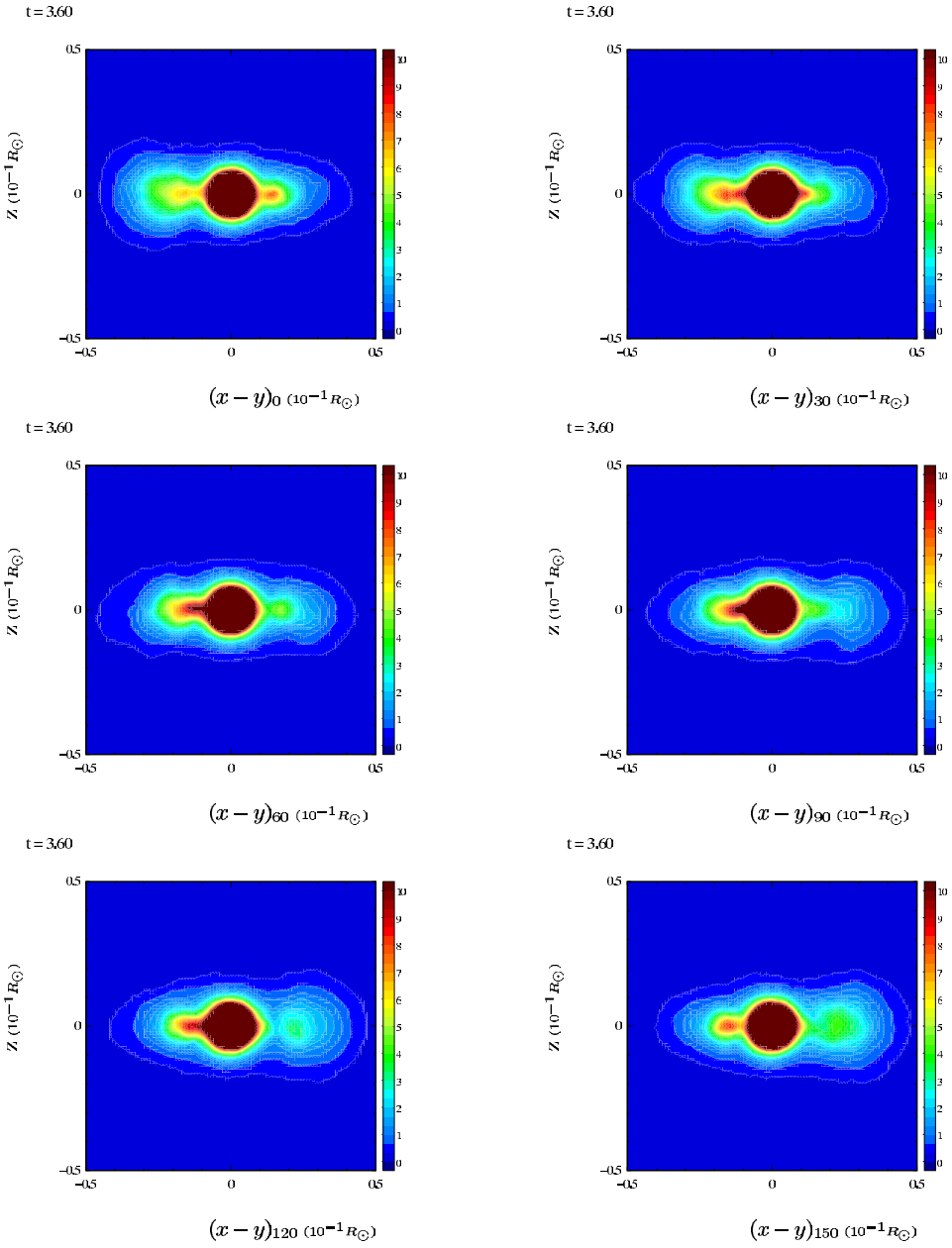

Fig. 9. Final axial density profiles for azimuthal angles ranging from 0° to 150° in 30° intervals, for the 0.4 + 1.2 $M_\odot$ binary system.

of He coalesces with a regular carbon–oxygen white dwarf nuclear reactions do not play a dominant role. Consequently, the formation of a thermonuclear supernovae during the merger process is quite unlikely even for this case in which the Coulomb barrier of the reacting nuclei is the smallest possible one although, again, it cannot be totally discarded.

3.2.4. Summary of the He+He, ONe+He and CO+He mergers

In Table 2 we show the global parameters obtained in this set of three simulations. The entries of this table are exactly the same of Table 1. Clearly, as it was found previously in Sect. 3.1, the peak temperature increases with the mass of the system. However, in any of the cases studied in this section the temperature is high enough to develop a strong thermonuclear runaway with the subsequent disruption of the system, even though – as already mentioned – the temperatures attained during the merger are most probably an overestimate of the real ones. Besides, and in agreement with the results presented in Sect. 3.1, the mass ejected during the merger is very small in all the cases, independently of the temperature, the masses of both the primary and the secondary and the chemical composition of the mergers. Particularly, it is interesting to note that in the case in which two He white dwarfs of equal masses are involved there is not any mass loss whatsoever. Finally, the total duration of the merger depends on the total mass of the coalescing system, being considerably smaller for the case in which a massive ONe white dwarf is involved.

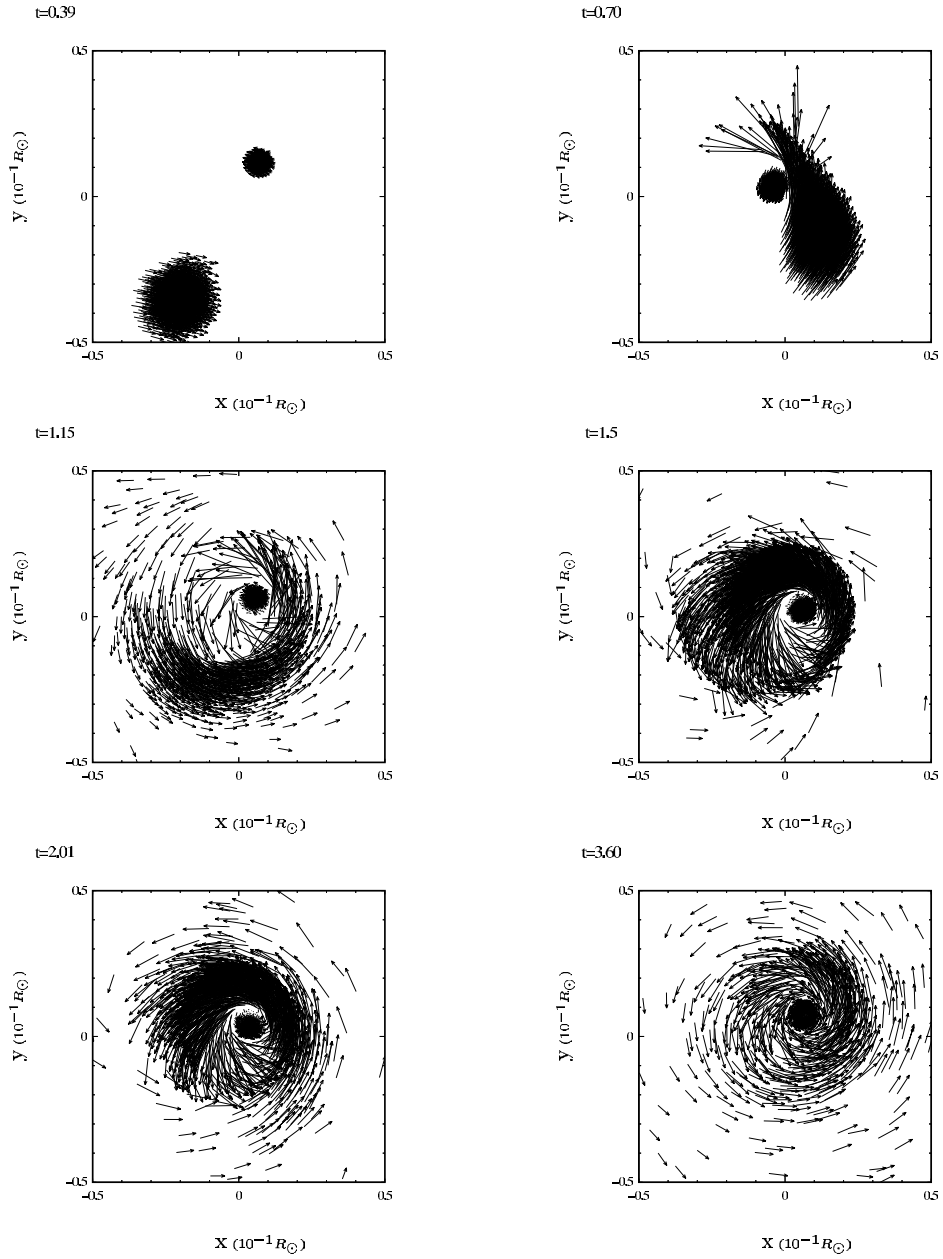

Fig. 10. Temporal evolution of the velocity field for the 0.4 + 1.2 $M_\odot$ binary system.

4. Discussion and conclusions

We have presented the results of the three-dimensional SPH calculations of the merging of white dwarfs in close binary systems. Our code incorporates a reduced nuclear network which has allowed us to follow the evolution of the system self-consistently for a significative range of masses of the components of the binary system. In particular, and in a first step, we have followed in detail the coalescence of three systems composed by 0.6 + 0.8 $M_\odot$, 0.6 + 1.0 $M_\odot$, and 0.8 + 1.0 $M_\odot$ white dwarfs. All these systems have in common that both white dwarfs are made of carbon and oxygen (the most abundant ones) and that the total mass of the system exceeds the Chandrasekhar limit. In all the cases studied so far we have found that the secondary is disrupted in a very short (dynamical) time scale. The final configuration consists in a central spherically symmetric object surrounded by a heavy Keplerian accretion disk with cylindrical symmetry supported by its own rotation. We have also found that the central object rotates as a rigid solid. We have argued that the rotational velocities of the central object are overestimated as a consequence of our treatment of the artificial viscosity which produces an unphysical shear. Hence, the rotational velocities of the central body obtained here are upper limits. Conversely, the rotational velocities of the Keplerian disk have been consequently underestimated. The maximum temperatures attained during the disruption of the secondary are in all cases close to 10^9 K. These maximum temperatures always occur in the most external, partially degenerate, shocked regions, and some material is burnt in the very first phases of the merger. However,

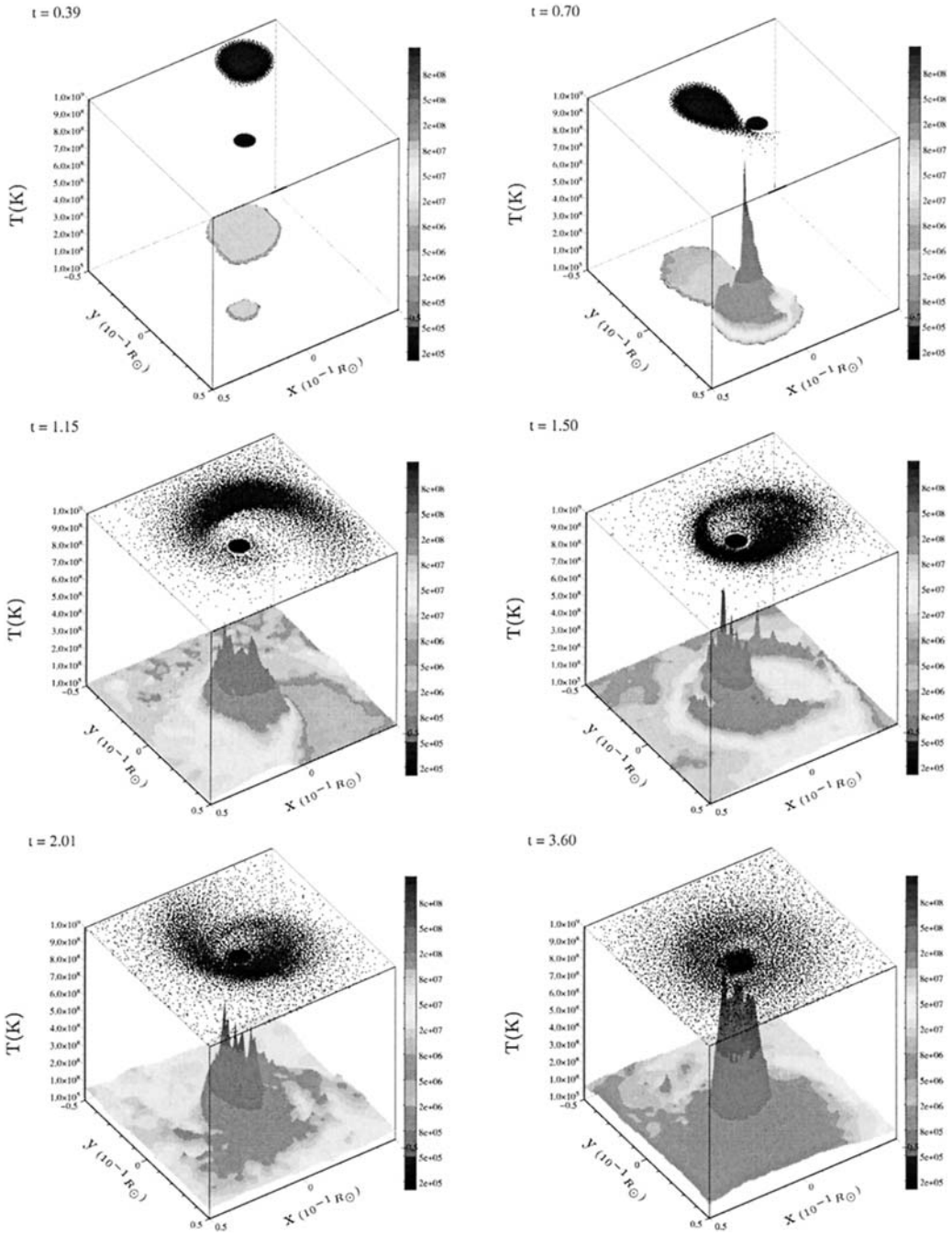

Fig. 11. Temporal evolution of the equatorial temperature contours for the 1.2 + 0.4 $M_{\odot}$ system.

Table 2. Global parameters of the simulations of the He+He, ONe+He and CO+He mergers.

Simulation	0.4+0.4	1.2+0.4	0.6+0.4
Ratio	1	1/3	2/3
$T_{\max}$ (K)	2.2×10^8	3.1×10^9	7.0×10^9
Mass of the particles ($M_{\odot}$)	4×10^{-5}	2×10^{-5}	2×10^{-5}
Expelled particles	0	1771	164
Expelled mass ($M_{\odot}$)	0	3.54×10^{-2}	3.32×10^{-3}
Fraction of the secondary expelled	0	8.9×10^{-2}	1.3×10^{-3}
Total expelled fraction	0	2.2×10^{-2}	3.3×10^{-3}
Duration (s)	600	180	569

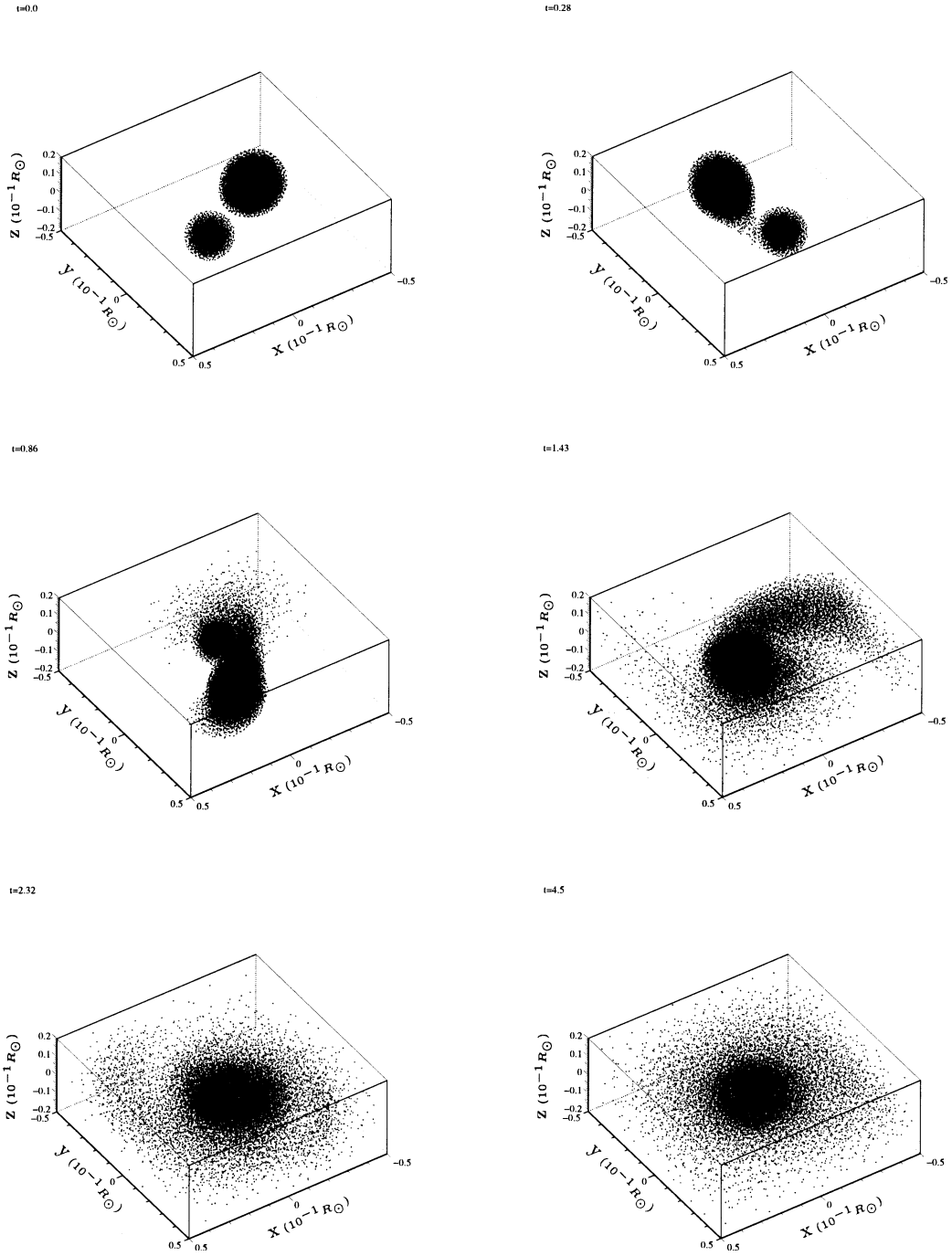

Fig. 12. Temporal evolution of the three dimensional positions of the SPH particles for the 0.6 + 0.4 $M_{\odot}$ system.

the rapid increase of the temperature rapidly lifts degeneracy and quenches the thermonuclear flash. Thus, nuclear reactions turn out to be unimportant during this phase of the evolution. Moreover, the maximum temperatures attained by the primary in our simulations are, probably, an overestimate of the temperature reached in real coalescing systems since some additional dissipation due to our treatment of the artificial viscosity is expected. Consequently, the possibility of a direct supernova explosion during the merger episode is quite unlikely although it cannot be completely ruled out. The ejected mass is always small ($\leq$0.5% of the total mass of the system) and comes primarily from the disrupted secondary. Our results, which have been obtained using a reduced nuclear network, are in good agreement with the results obtained by Segretain et al. (1997), who neglected the effects of nuclear reactions. Therefore, according to the analysis of Segretain et al. (1997), we expect that the heavy accretion disk is likely to loose mass and angular momentum.

In a second step, we have also explored which would be the effect of the chemical composition of the coalescing white dwarfs. To this regard we have conducted a series of three additional numerical simulations in which white dwarfs made of helium, carbon–oxygen and oxygen–neon are involved. Their respective masses are 0.4+0.4 $M_{\odot}$, 0.6+0.4 $M_{\odot}$, and 1.2+0.4 $M_{\odot}$.

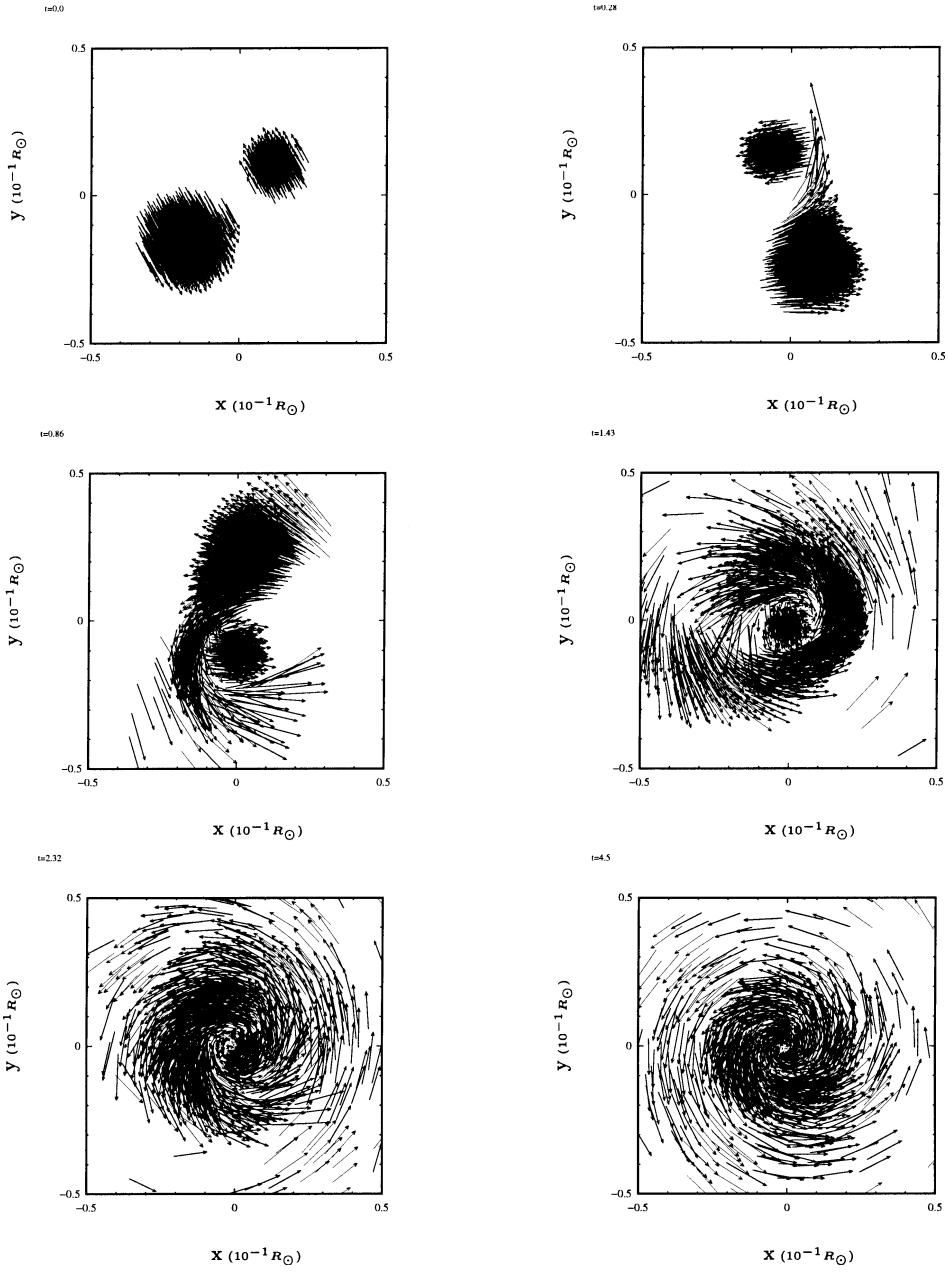

Fig. 13. Temporal evolution of the velocities projected in the orbital plane of the SPH particles for the $0.6 + 0.4\ M_\odot$ system.

We have found that for all these cases, except for the first one, the final configuration is quite similar to what was found for the case of carbon–oxygen white dwarfs. The final remnant for these two cases consists in a central rotating object and a heavy accretion disk. For the case in which two equal-mass He white dwarfs are involved the remnant has cylindrical symmetry. We have found that consists in a central spinning region surrounded by an extended accretion disk, again rotationally supported. The temperatures attained during the most violent phases of the merger are also high in all three cases but, again, nuclear reactions do not significantly alter the evolution of the systems. In particular, no explosion has been obtained in none of the three cases. Similarly the ejected masses are small in all the three cases.

According to our findings the following possibilities arise. Firstly, it is clear that a type Ia thermonuclear supernova is not likely to be the outcome as a direct consequence of the coalescence. However although the possibility of a strong thermonuclear flash during the merger is unlikely, the final result of our simulations allows for stable accretion onto the primary and, hence, a supernova explosion cannot be discarded to occur at late stages. The second possible scenario in which the coalescence of two white dwarfs bears important consequences is the possibility that the anomalous X-ray pulsar 1E2259+586 could be the consequence of such a merging episode. According to Paczyński (1990) the age of this pulsar is $\sim 2 \times 10^4$ yr and its rotation must be high – the total rotational kinetic energy stored in the central object should be $\sim 10^{50}$ ergs. In order for our simulations to obtain such a high rotational energy all the mass in the merger should be accumulated onto the central object. This, as we have shown, turns out to be very unlikely since very high accretion rates – of the order of $10^{-5}\ M_\odot\ \mathrm{yr}^{-1}$ – are

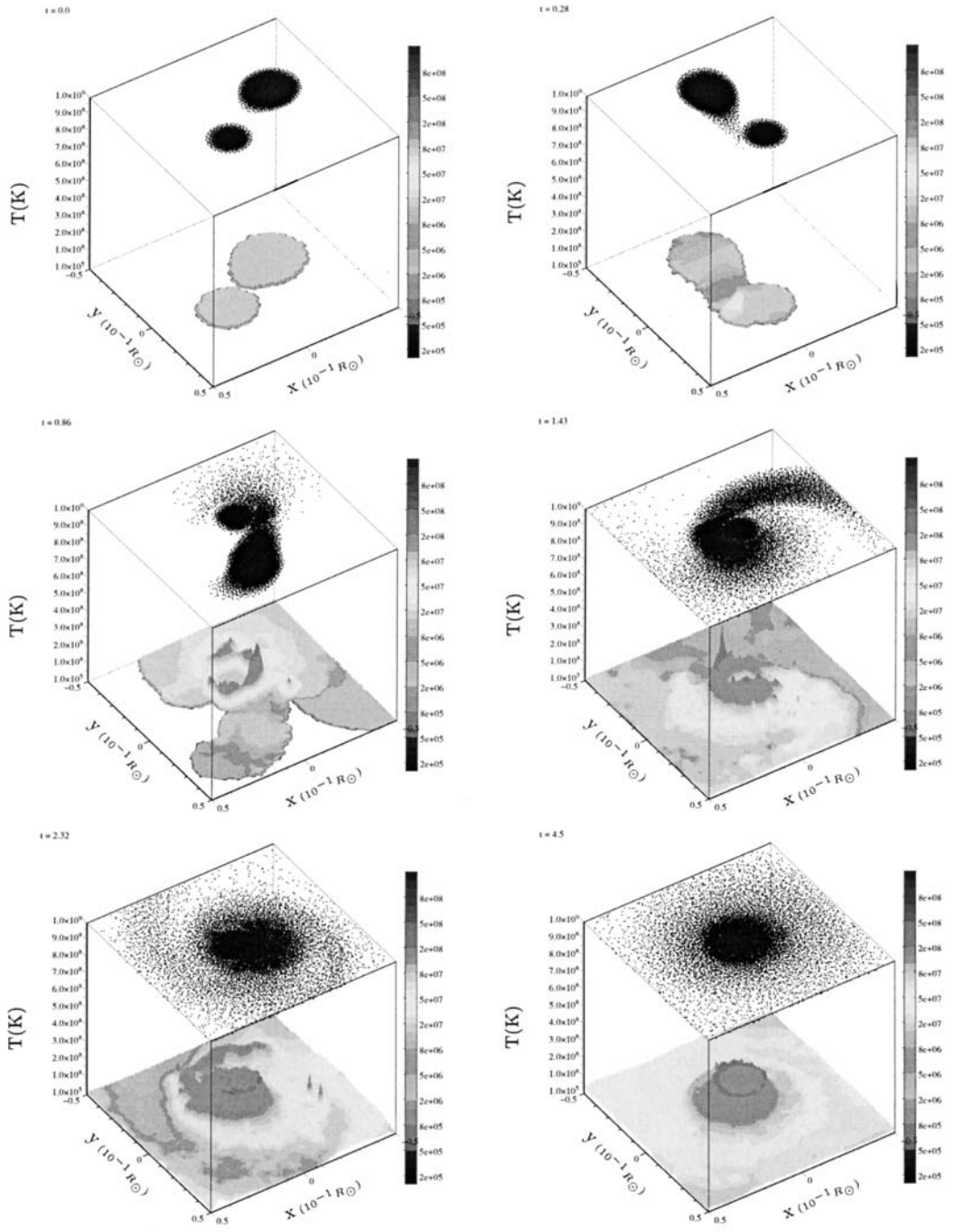

Fig. 14. Temporal evolution of the equatorial temperature contours for the 0.6 + 0.4 $M_\odot$ system.

needed. Moreover during the accretion phase there would be two competing process. On the one hand, the increase in the rotational velocity due to the transfer of angular momentum from the disk to the primary, and, on the other, the decrease in the rotational velocity due to the magnetic dipole radiation emission. The former should be dominant at the beginning of the accretion phase in order to produce a rapidly spinning pulsar, whereas the later should be dominant in a subsequent phase in order to allow for the observed increase in the period, leading to even larger accretion rates. Finally, the mass of the pulsar ($\simeq$1.3 $M_\odot$) also requires that a large fraction of the mass and, hence, of angular momentum is lost from the system. Clearly our simulations leave still some room for such a fine tuning of all these processes, but this possibility remains quite unlikely unless the resulting object first accretes enough matter to start carbon burning off-center (García–Berro et al. 1997) to form an ONe white dwarf and, later, to form a neutron star through the Accretion Induced Collapse scenario (Gutiérrez et al. 1996). In this last process a strong neutrino driven wind could remove mass enough to allow for the formation of a pulsar with the required mass. Finally, the other possibility is the formation of a hot massive white dwarf. The final result of the merger is always a hot massive object. Our simulations, which include a nuclear reaction network, are in agreement with the results

of Segretain et al. (1997), which were computed without such a nuclear network. Thus, their conclusions in this regard remain valid. In particular, the possibility that the three massive white dwarfs PG 0136+251, PG 1658+441 and GD 50 could be the result of a merger is still valid, despite the large fraction of angular momentum (∼80%) that must be removed from the system during a cooling time scale.

Finally, our results are relevant as well for the understanding of the so-called subdwarf B (sdB) objects. For many years the evolutionary origins of subdwarf B stars remained a mistery, but as first suggested by Iben (1990) there are solid reasons to suspect that most if not all sdB stars are the result of the coalescence of white dwarfs in a binary system. Most sdB stars have spectra that show helium abundances depleted to a lesser or greater extent. This is attributed to gravitational settling. However, among sdB stars there is a specific class of objects which shows relatively strong He features in their spectra. It has been recently proposed (Aznar Cuadrado & Jeffery 2002) that these objects are presumably the result of the coalescence of two He white dwarfs (Saio & Jeffery 2000), although the possibility of a He+CO white dwarf merger has not yet been discarded. We have simulated both possibilities. Although our simulations do not allow us to follow the long term evolution of the resulting objects it is clear that they provide a ground for more elaborated studies. Finally we would like to stress that in order to obtain definite answers to all these issues an improved treatment of the artificial viscosity is needed. In particular Morris & Monaghan (1997) have proposed a switch to reduce the excessive shear produced by the artificial viscosity of Balsara (1995). The inclusion of such a switch would allow one to compute what fraction of the total angular momentum is transferred to the disk and what fraction is transferred to the central object. Another possibility would be to incorporate the Riemann solver designed by Monaghan (1997). Such possibilities are now under study.

Acknowledgements. Part of this work was supported by the Spanish MCYT grants AYA2000–1785 and AYA2002-04094-C03-01/02, and by the CIRIT. We would also like to acknowledge our anonymous referee for very valuable comments and suggestions.

References

Abramovici, A., Althouse, W. E., Drever, R. W. P., et al. 1992, Science, 256, 325
Aznar Cuadrado, R., & Jeffery, C. S. 2002, A&A, 369, 994
Balsara, D. 1995, J. Comp. Phys., 121, 357
Barnes, J., & Hut, P. 1986, Nature, 324, 446
Benz, W. 1990, in The numerical modelling of Nonlinear stellar Pulsations, ed. J. Buchler (Dordrecht: Kluwer Academic Publishers), 269
Benz, W., Cameron, A. G. W., & Bowers, R. L. 1989, in White Dwarfs, ed. G. Wegner (Berlin: Springer-Verlag Berlin), Proc. of IAU Coll., 114, 511
Benz, W., Bowers, R. L., Cameron, A. G. W., & Press, W. 1990, ApJ, 348, 647
Benz, W., Hills, J. G., & Thielemann, F.-K. 1989, ApJ, 342, 986
Bragaglia, A., Greggio, L., Renzini, A., & D'Odorico, S. 1990, ApJ, 365, L13
Clemens, M. J. 1974, ApJ, 194, 709
Evans, C. R., Iben, I. Jr., & Smarr, L. 1987, ApJ, 323, 129
García–Berro, E., Ritossa, C., & Iben, I. Jr. 1997, ApJ, 485, 765
Gutiérrez, J., García–Berro, E., Iben, I. Jr., et al. 1996, ApJ, 459, 701
Gingold, R. A., & Monaghan, J. J. 1977, MNRAS, 181, 375
Iben, I. 1990, ApJ, 353, 215
King, A. R., Pringle, J. E., & Wickramasinghe, D. T. 2001, MNRAS, 320, L45
Lucy, L. B. 1977, AJ, 82, 1013
Marsh, T. R. 1995, MNRAS, 275, L1
Marsh, T. R., Dhillon, V. S., & Duck, S. R. 1995, MNRAS, 275, 828
Maxted, P. F. L., & Marsh, T. R. 1999, MNRAS, 307, 122
Maxted, P. F. L., Marsh, T. R., & North 2000, MNRAS, 317, L41
Monaghan, J. J. 1997, J. Comp. Phys., 136, 298
Monaghan, J. J., & Lattanzio, J. C. 1985, A&A, 149, 135
Monaghan, J. J., & Gingold, R. 1983, J. Comp. Phys., 52, 374
Morris, J. P., & Monaghan, J. J. 1997, J. Comp. Phys., 136, 41
Mochkovitch, R., & Livio, M. 1989, A&A, 209, 111
Mochkovitch, R., & Livio, M. 1990, A&A, 236, 378
Nelemans, G., Yungelson, L. R., Portegies Zwart, S. F., & Verbunt, F. 2001a, A&A, 365, 491
Nelemans, G., Portegies Zwart, S. F., Verbunt, F., & Yungelson, L. R. 2001b, A&A, 368, 939
Ostriker, J. P., & Mark, J. W. K. 1968, ApJ, 151, 1075
Paczyński, B. 1990, ApJ, 365, L9
Rauscher, T., & Thielemann, F.-K. 2000, Atom. Data & Nucl. Data Tables, 75, 1
Rosswog, S., Davies, M. B., Thielemann, F.-K., & Piran, T. 2000, A&A, 360, 171
Rosswog, S., & Davies, M. B. 2002, MNRAS, 334, 481
Saio, H., & Jeffery, C. S. 2000, MNRAS, 313, 671
Segretain, L., Chabrier, G., & Mochkovitch, R. 1997, ApJ, 481, 355
Schmidt, G. D., Bergeron, P., Liebert, J., & Saffer, R. A. 1992, ApJ, 394, 603
Seto, N. 2002, MNRAS, 333, 469
Yungelson, L. R., Livio, M., Tutukov, A. V., & Saffer, R. A. 1994, ApJ, 420, 336